doi:10.1038/nature13156

A Sedna-like body with a perihelion of 80 astronomical units

Chadwick A. Trujillo[1]* & Scott S. Sheppard[2]*

The observable Solar System can be divided into three distinct regions: the rocky terrestrial planets including the asteroids at 0.39 to 4.2 astronomical units (AU) from the Sun (where 1 AU is the mean distance between Earth and the Sun), the gas giant planets at 5 to 30 AU from the Sun, and the icy Kuiper belt objects at 30 to 50 AU from the Sun. The 1,000-kilometre-diameter dwarf planet Sedna was discovered ten years ago and was unique in that its closest approach to the Sun (perihelion) is 76 AU, far greater than that of any other Solar System body[1]. Formation models indicate that Sedna could be a link between the Kuiper belt objects and the hypothesized outer Oort cloud at around 10,000 AU from the Sun[2–6]. Here we report the presence of a second Sedna-like object, 2012 VP_{113}, whose perihelion is 80 AU. The detection of 2012 VP_{113} confirms that Sedna is not an isolated object; instead, both bodies may be members of the inner Oort cloud, whose objects could outnumber all other dynamically stable populations in the Solar System.

The inner Oort cloud objects probably formed on nearly circular orbits, allowing them to accumulate mass efficiently[6–9], and were later perturbed into the eccentric orbits we see today. We define an inner Oort cloud object as a body whose orbit is not readily formed with the known mass in the Solar System. This typically means a perihelion greater than 50 AU (beyond the range of significant Neptune interaction) and a semi-major axis in the range 150 AU $< a <$ 1,500 AU. At above 1,500 AU objects may be considered to be in the outer Oort cloud, as galactic tides start to become important in the formation process[10]. Sedna and 2012 VP_{113} are the clearest examples of inner Oort cloud objects because they do not interact significantly with any of the known planets owing to their extremely distant perihelia (Fig. 1 and Table 1).

There are two main models for inner Oort cloud object formation. In the first model, planet-sized object(s) in the outer Solar System may perturb objects from the Kuiper belt outward to inner-Oort-cloud orbits. These planet-sized objects could either remain (unseen) in the Solar System[5,11] or have been ejected from the Solar System during the creation of the inner Oort cloud[12]. In the second model, close stellar encounter(s) can create the inner Oort cloud objects, possibly within the first ten million years (Myr) of the Sun's life, when it resided within its birth cluster[1,3,4,11,13–17]. The outer Oort cloud objects could be created from galactic tides[18], but the more tightly bound inner Oort cloud objects are difficult to create without a close stellar encounter[19]. A third, less explored, model is that the inner Oort cloud objects are captured extrasolar planetesimals lost from other stars that were in the Sun's birth cluster[2,3,20]. Each theory of inner Oort cloud object formation predicts different orbital configurations for the population. Therefore, as more inner Oort cloud objects are discovered, their orbits will provide strong constraints on the inner Oort cloud object formation models and thus our Solar System's evolution.

To place constraints on the inner Oort cloud object population, we constructed a simple simulation of the observational biases affecting our survey (Methods). We find three basic results from this analysis: (1) there appears to be a paucity of inner Oort cloud objects with perihelia in the range 50–75 AU, suggesting that the inner Oort cloud object population could increase with $q > 75$ AU; (2) the existence of 2012 VP_{113} means that the inner Oort cloud object population must reach down to fairly small semi-major axes of about 250 AU; and (3) there are no observational biases that can explain the clustering of the argument of perihelion (ω) near 340° for inner Oort cloud objects and all objects with semi-major axes greater than 150 AU and perihelia greater than Neptune.

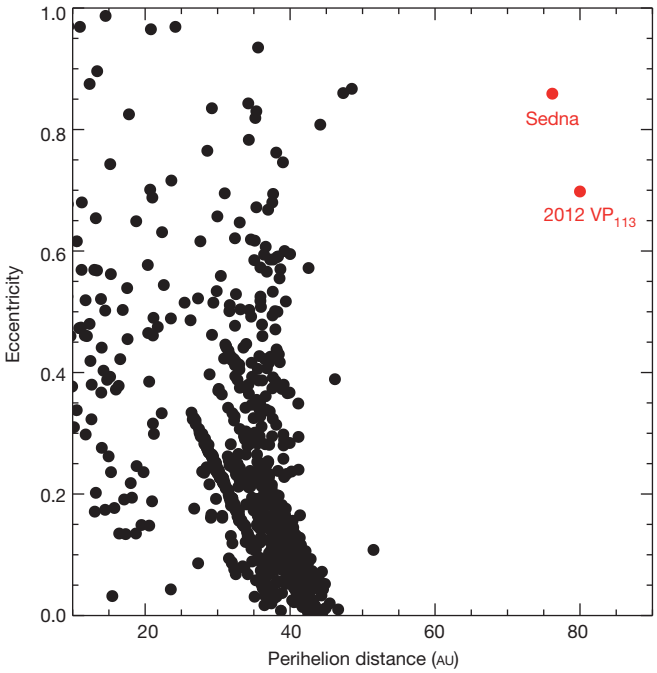

Figure 1 | Sedna and 2012 VP_{113} are clear dynamical outliers in the Solar System. Eccentricity versus perihelion distance for the approximately 1,000 minor planets with well-determined (multi-year) orbits beyond 10 AU are depicted. There are no known objects with closest-approach distances (perihelia, q) between 55 AU and 75 AU, even though such objects would be closer, and should therefore be brighter and easier to detect than Sedna or 2012 VP_{113}. This suggests there may be a paucity of inner Oort cloud objects with $q < 75$ AU. The perihelia of Sedna and 2012 VP_{113} are much too distant from Neptune (30 AU) for their existence to be explained by the known mass in the Solar System. All error bars are smaller than the data symbols.

Although our survey was sensitive to objects from 50 AU to beyond 300 AU, no objects were found with perihelion distances between 50 AU and 75 AU, where objects are brightest and easiest to detect. This was true for the original survey that found Sedna[1] and the deeper follow-up survey[21]. Figure 2 illustrates this—most simulated objects (and the real objects Sedna and 2012 VP_{113}) are found near the inner edge of the population. If the inner Oort cloud objects had a minimum perihelion of 50 AU and followed a size distribution like that of the large end of all known

[1]Gemini Observatory, 670 North A'ohoku Place, Hilo, Hawaii 96720, USA. [2]Department of Terrestrial Magnetism, Carnegie Institution for Science, 5241 Broad Branch Road NW, Washington, DC 20015, USA.
*These authors contributed equally to this work.

©2014 Macmillan Publishers Limited. All rights reserved

Table 1 | The orbital elements of the inner Oort cloud objects

Object	q (AU)	a (AU)	e	i (deg)	Ω (deg)	ω (deg)	t_p (JD)	Epoch (JD)
2012 VP_{113}	80	266	0.698	24.051	90.806	293	2,443,300	2,455,857.1
Sedna	76.23	542	0.8593	11.92840	144.466	311.01	2,479,197	2,456,400.5

The barycentric elements for 2012 VP_{113} and the heliocentric elements for Sedna (from the NASA Jet Propulsion Laboratory Horizons tool for dwarf planets http://ssd.jpl.nasa.gov/?horizons) are given as semi-major axis (a), eccentricity (e), inclination (i), longitude of ascending node (Ω), argument of perihelion (ω), and perihelion distance (q), which has been derived from a and e. Time of perihelion (t_p) and epoch are specified in terms of the Julian date (JD). The precision to which quantities are known is reflected in the number of significant digits. We define inner Oort cloud objects as having $q > 50$ AU and 150 AU $< a <$ 1,500 AU (see main text).

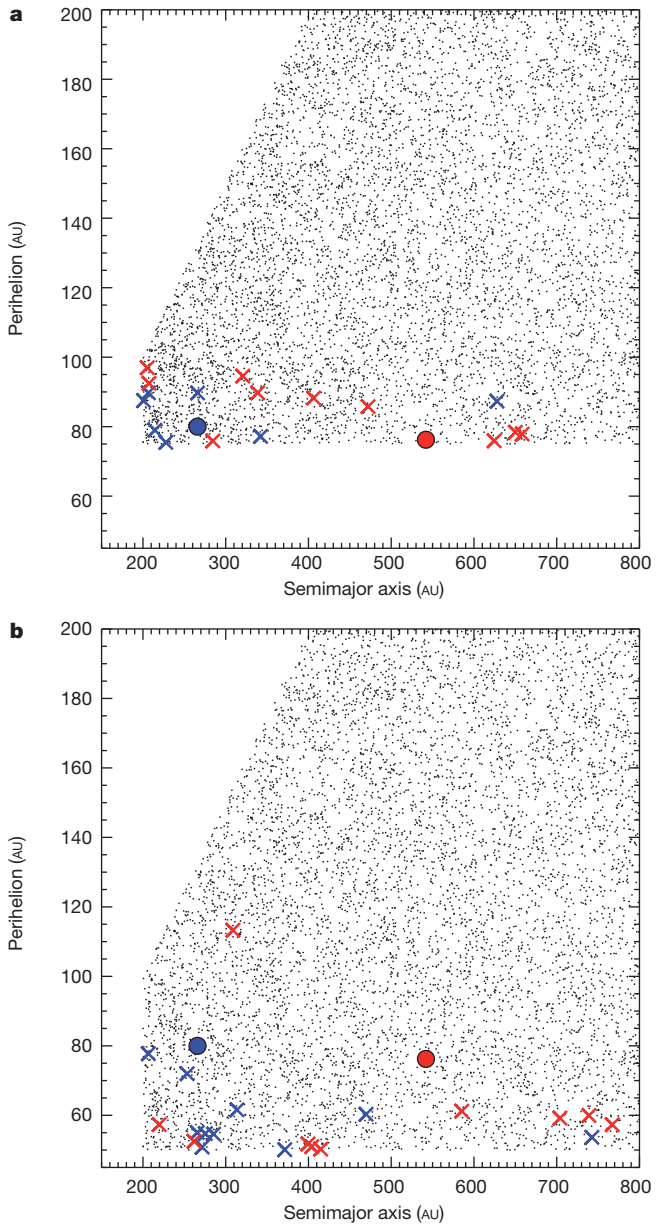

Figure 2 | Results from the observational bias simulation. The simulated inner Oort cloud objects (dots) are shown, along with the simulated detections in our survey (blue crosses) and the most sensitive all-sky survey so far, which re-detected Sedna[21] (red crosses) for two different inner Oort cloud object models: our favoured model (**a**) and a comparison model (**b**). We have displayed ten simulated survey realizations per survey. The true values for Sedna and 2012 VP_{113} are shown as red and blue circles, respectively, both with error bars much smaller than the plot symbol (there are no error bars associated with all other symbols, which describe simulated data). There is one difference between the two models, the minimum perihelion for the underlying population (75 AU in **a** versus 50 AU in **b**). Our observational results favour the model in **a** because both Sedna and 2012 VP_{113} were found within a few AU of their perihelion. This indicates that the inner Oort cloud objects may have increasing numbers with increasing distance.

small-body reservoir distributions[22,23] ($q' = 5$), there would be only a 1% chance of finding 2012 VP_{113} and Sedna with perihelion greater than 75 AU and no objects with perihelion less than 75 AU. Therefore, we conclude that there are few (although probably not zero) inner Oort cloud objects in the 50–75 AU region. Some stellar encounter models that include the capture of extrasolar material predict a strong inner edge to the perihelion distribution of objects, which is consistent with our observations[2].

Our simulation suggests that the inner Oort cloud contains about 1/80th of an Earth mass of material for our favoured $q' = 5$ model, although this can vary based on the assumed size distribution (Methods and Extended Data Table 1). This is similar to that of the Kuiper belt objects (KBOs), which have about 1/100th of an Earth mass of material[22]. We estimate that about $430^{+400}_{-240}(1\sigma)$ inner Oort cloud objects brighter than $r = 24.3$ remain undiscovered throughout the sky. In addition, $900^{+800}_{-500}(1\sigma)$ bodies are expected with diameter larger than 1,000 km (most of which are extremely distant), which is statistically consistent with detailed model estimates based only on the discovery of Sedna[21]. Our simulations assume that the inner Oort cloud objects are longitudinally symmetric, but it is interesting that both 2012 VP_{113} and Sedna were found at similar sky locations. If further inner Oort cloud object discoveries prove this effect to be statistically significant, this would strongly constrain inner Oort cloud object formation models.

Both Sedna and 2012 VP_{113} have similar arguments of perihelion ($\omega = 311°$ and 293°, respectively). The orbital element ω describes the angle between the point of perihelion and where a body's orbit crosses the celestial plane. Surprisingly, this ω similarity is shared for all known objects with semi-major axes greater than 150 AU and perihelia greater than that of Neptune ($\omega \approx 340° \pm 55°$; see Fig. 3, Extended Data Fig. 1 and Extended Data Table 2). These extreme scattered disk objects may have a similar origin to Sedna or 2012 VP_{113} but their much lower perihelia ($q < 49$ AU) allow their existence to be explained through resonant interactions with Neptune, except for 2004 VN_{112}, 2010 GB_{174} and possibly 2000 CR_{105} (refs 10, 24–27). We find that this ω clustering cannot be due to observational bias for two reasons: (1) any bias for $\omega = 0°$ is the same as the bias for $\omega = 180°$; and (2) the surveys that have found the objects with clustered ω were often off-ecliptic or all-sky surveys, which would not have a bias for either $\omega = 0°$ or 180° (Methods). Thus, we conclude that the ω clustering is a real effect.

The Lidov–Kozai effect is the best known dynamical mechanism for constraining the ω of a minor planet[28]. This three-body interaction can create outer Oort cloud objects with ω preferentially near 0° and 180° early in the history of the Solar System when the Sun was still among its nascent cohort of perturbing stars[29]. This cannot explain the $\omega \approx 0°$ trend today, because ω circulates owing to the presence of the giant planets. By numerically simulating the effect of the known mass in the Solar System on the inner Oort cloud objects, we confirmed that inner Oort cloud objects should have random ω (Methods). This suggests that a massive outer Solar System perturber may exist and restricts ω for the inner Oort cloud objects. We numerically simulated the effect of a super-Earth-mass body at 250 AU and found that ω for inner Oort cloud objects librated around $0° \pm 60°$ for billions of years (see Extended Data Figs 2 and 3). This configuration is not unique and there are many possibilities for such an unseen perturber. A super-Earth-mass body at 250 AU with very low albedo would be fainter than current all-sky survey detection limits, as would larger and more distant perturbers[30].

©2014 Macmillan Publishers Limited. All rights reserved

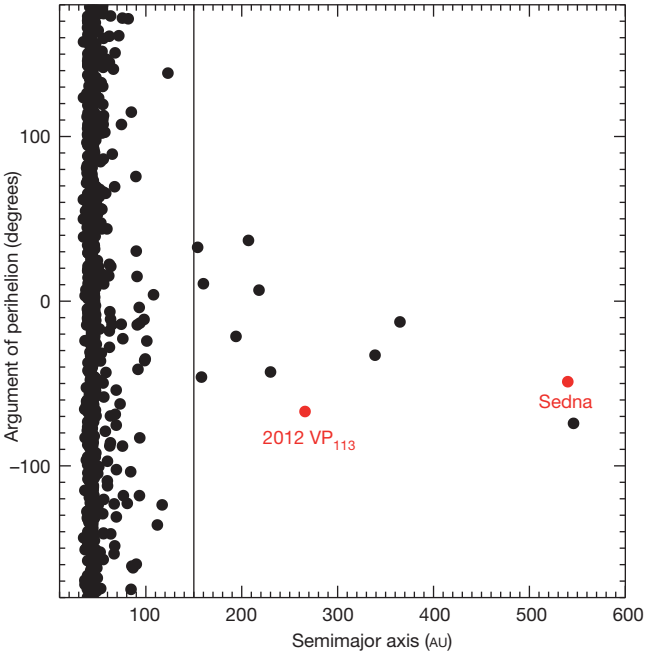

Figure 3 | The argument of perihelion for distant objects clusters about 0°. All minor planets with perihelion greater than 30 AU as a function of semi-major axis are shown. All bodies with semi-major axis greater than the line at 150 AU show a pronounced concentration near $\omega \approx 0°$. Errors on these orbital elements are much smaller than the plotted symbols. This figure appears in histogram form in Extended Data Fig. 1.

Although such a perturber could keep the ω near 0°, how objects initially obtained $\omega \approx 0°$ and not 180° is unknown. Stochastic events, such as a single strong stellar encounter or rogue planet could produce such asymmetric populations. A strong stochastic encounter could also produce the low semi-major axis of 2012 VP_{113}. It is possible that the ω clustering indicates that all $q > 30$ AU and $a > 150$ AU bodies formed by a similar process, although bodies on elliptical orbits with q less than approximately 45 AU can be explained by Neptune interactions. Models of galactic tides have difficulty producing inner Oort cloud objects having low semi-major axes (like Sedna) in the absence of stellar encounters[19] so the even lower semi-major axis of 2012 VP_{113} makes tides extremely unlikely. If the inner Oort cloud objects were created from the gravitational tide within our Sun's birth cluster, the low semi-major axis of 2012 VP_{113} constrains the birth cluster to have been a moderate 10,000 solar masses per cubic parsec or more, depending on the cluster model assumed[15,29]. The moderately red optical colours observed for 2012 VP_{113} (Methods and Extended Data Table 3) are consistent with formation in the gas giant region and not in the ultra-red dominated classical Kuiper belt. Assuming a moderate albedo, 2012 VP_{113} is 450 km in diameter, large enough to be considered a dwarf planet if it is composed largely of ice.

METHODS SUMMARY

For this work, we conducted two main observational investigations. First, we surveyed 52 square degrees of sky for new inner Oort cloud objects using the Dark Energy Camera (DECam) at the Cerro Tololo Inter-American Observatory (CTIO) 4-m telescope. Each patch of sky was imaged three times with 1.5 h to 2 h between images, giving us the ability to detect the motion of objects beyond 300 AU when compared to background stars. Analysis software aided our search for moving objects. After its discovery at the CTIO 4-m telescope, we measured the position and colour of 2012 VP_{113} using the Magellan 6.5-m telescope, completing the data collection portion of our project. We then created an observational bias simulation that simulated our discovery process to place constraints on the underlying number and orbital distribution of inner Oort cloud objects. This produces order-of-magnitude results for the number of inner Oort cloud objects whose basic parameters are poorly constrained because so few are known. Finally, after identifying the unusual nature of the ω distribution, we simulated the inner Oort cloud objects and the other minor planets with semi-major axes greater than 150 AU and perihelion greater than 30 AU to explore the long-term behaviour of ω for different hypothetical planetary masses in the Solar System. These methods are described in greater detail in the Methods section.

Online Content Any additional Methods, Extended Data display items and Source Data are available in the online version of the paper; references unique to these sections appear only in the online paper.

Received 11 October 2013; accepted 10 February 2014.

1. Brown, M. E., Trujillo, C. & Rabinowitz, D. Discovery of a candidate inner Oort cloud planetoid. *Astrophys. J.* **617,** 645–649 (2004).
2. Morbidelli, A. & Levison, H. F. Scenarios for the origin of the orbits of the trans-Neptunian objects 2000 CR_{105} and 2003 VB_{12} (Sedna). *Astron. J.* **128,** 2564–2576 (2004).
3. Kenyon, S. J. & Bromley, B. C. Stellar encounters as the origin of distant Solar System objects in highly eccentric orbits. *Nature* **432,** 598–602 (2004).
4. Melita, M. D., Larwood, J. D. & Williams, I. P. Sculpting the outer Edgeworth Kuiper belt: stellar encounter followed by planetary perturbations. *Icarus* **173,** 559–573 (2005).
5. Gomes, R. S., Matese, J. J. & Lissauer, J. J. A distant planetary-mass solar companion may have produced distant detached objects. *Icarus* **184,** 589–601 (2006).
6. Levison, H. F. & Morbidelli, A. Models of the collisional damping scenario for ice-giant planets and Kuiper belt formation. *Icarus* **189,** 196–212 (2007).
7. Goldreich, P., Lithwick, Y. & Sari, R. Final stages of planet formation. *Astrophys. J.* **614,** 497–507 (2004).
8. Batygin, K., Brown, M. E. & Betts, H. Instability-driven dynamical evolution model of a primordially five-planet outer Solar System. *Astrophys. J.* **744,** L3 (2012).
9. Nesvorný, D. & Morbidelli, A. Statistical study of the early Solar System's instability with four, five, and six giant planets. *Astron. J.* **144,** 117 (2012).
10. Gomes, R. S., Gallardo, T., Fernández, J. A. & Brunini, A. On the origin of the high-perihelion scattered disk: the role of the Kozai mechanism and mean motion resonances. *Celestial Mech. Dyn. Astron.* **91,** 109–129 (2005).
11. Soares, J. S. & Gomes, R. S. Comparison of forming mechanisms for Sedna-type objects through an observational simulator. *Astron. Astrophys.* **553,** A110 (2013).
12. Gladman, B. & Chan, C. Production of the extended scattered disk by rogue planets. *Astrophys. J.* **643,** L135–L138 (2006).
13. Ida, S., Larwood, J. & Burkert, A. Evidence for early stellar encounters in the orbital distribution of Edgeworth-Kuiper belt objects. *Astrophys. J.* **528,** 351–356 (2000).
14. Brasser, R. A two-stage formation process for the Oort comet cloud and its implications. *Astron. Astrophys.* **492,** 251–255 (2008).
15. Brasser, R., Duncan, M. J., Levison, H. F., Schwamb, M. E. & Brown, M. E. Reassessing the formation of the inner Oort cloud in an embedded star cluster. *Icarus* **217,** 1–19 (2012).
16. Dukes, D. & Krumholz, M. R. Was the Sun born in a massive cluster? *Astrophys. J.* **754,** 56 (2012).
17. Pfalzner, S. Early evolution of the birth cluster of the solar system. *Astron. Astrophys.* **549,** A82 (2013).
18. Adams, F. C. The birth environment of the Solar System. *Annu. Rev. Astron. Astrophys.* **48,** 47–85 (2010).
19. Kaib, N. A., Roškar, R. & Quinn, T. Sedna and the Oort cloud around a migrating Sun. *Icarus* **215,** 491–507 (2011).
20. Levison, H. F., Duncan, M. J., Brasser, R. & Kaufmann, D. E. Capture of the Sun's Oort cloud from stars in its birth cluster. *Science* **329,** 187–190 (2010).
21. Schwamb, M. E., Brown, M. E., Rabinowitz, D. L. & Ragozzine, D. Properties of the distant Kuiper belt: results from the Palomar Distant Solar System Survey. *Astrophys. J.* **720,** 1691–1707 (2010).
22. Petit, J.-M. *et al.* The Canada-France Ecliptic Plane Survey—full data release: the orbital structure of the Kuiper belt. *Astron. J.* **142,** 131 (2011).
23. Schwamb, M. E., Brown, M. E. & Fraser, W. C. The small numbers of large Kuiper belt objects. *Astron. J.* **147,** 2 (2014).
24. Gladman, B. *et al.* Evidence for an extended scattered disk. *Icarus* **157,** 269–279 (2002).
25. Gomes, R. S., Fernández, J. A., Gallardo, T. & Brunini, A. in *The Solar System Beyond Neptune* (eds Barucci, M. A., Boehnhardt, H., Cruikshank, D. P., Morbidelli, A. & Dotson, R.) 259–273 (2008).
26. Becker, A. C. *et al.* Exploring the outer Solar System with the ESSENCE Supernova Survey. *Astrophys. J.* **682,** L53–L56 (2008).
27. Chen, Y.-T. *et al.* Discovery of a new member of the inner Oort cloud from the Next Generation Virgo Cluster Survey. *Astrophys. J.* **775,** L8 (2013).
28. Kozai, Y. Secular perturbations of asteroids with high inclination and eccentricity. *Astron. J.* **67,** 591 (1962).
29. Brasser, R., Duncan, M. J. & Levison, H. F. Embedded star clusters and the formation of the Oort cloud. *Icarus* **184,** 59–82 (2006).
30. Sheppard, S. S. *et al.* A southern sky and galactic plane survey for bright Kuiper belt objects. *Astron. J.* **142,** 98 (2011).

Acknowledgements We thank the Dark Energy Camera (DECam) team for obtaining observations during DECam commissioning, D. Norman for scheduling the November 2012 DECam observations, and D. Norman, A. Kunder and K. Holhjem for queue observing in November. T. Abbott and F. Valdes were very helpful during our December 2012 DECam observations. This project used data obtained with DECam, which was

©2014 Macmillan Publishers Limited. All rights reserved

constructed by the Dark Energy Survey collaborating institutions. Observations were in part obtained at the Cerro Tololo Inter-American Observatory, National Optical Astronomy Observatory, which is operated by the Association of Universities for Research in Astronomy, under contract with the National Science Foundation. This paper includes data gathered with the 6.5-m Magellan telescopes located at Las Campanas Observatory, Chile. This research was funded by NASA Planetary Astronomy grant NNX12AG26G and has also been supported by the Gemini Observatory, which is operated by the Association of Universities for Research in Astronomy, Inc., on behalf of the international Gemini partnership of Argentina, Australia, Brazil, Canada, Chile and the USA.

Author Contributions C.T. created the moving object detection program for image analysis, developed the discovery statistic simulations, and is the principal investigator of the NASA grant supporting the project. S.S. obtained the telescope time, planned and performed the observations, analysed the data (including the colour measurements) and estimated the inner Oort cloud object orbital evolution using the Mercury integrator.

Author Information Reprints and permissions information is available at www.nature.com/reprints. The authors declare no competing financial interests. Readers are welcome to comment on the online version of the paper. Correspondence and requests for materials should be addressed to C.T. (trujillo@gemini.edu).

©2014 Macmillan Publishers Limited. All rights reserved

METHODS

Discovery survey. In our survey, we imaged 52 square degrees of sky using DECam[31] at CTIO, which has the largest field of view (2.7 square degrees) of any 4 m or larger telescope. This work covers our survey from November and December 2012, which was comprised of 15 fields with mean ecliptic latitude -12.9° and 4 fields with mean ecliptic latitude -35.5°. We estimate that our survey is sensitive to 95% of objects as faint as red magnitude $m_r = 24.3$ with a 50% detection efficiency at about $m_r = 24.5$. Solar System objects are found by measuring their apparent motion relative to distant, stationary background stars. Our observational strategy is to observe each field three times with 1.5 h to 2 h between each image. Our ~3.5-h time base corresponds to about 1.6 arcseconds of motion for a body at 300 AU, which is easily visible in the ~1-arcsecond full-width-at-half-maximum image quality of DECam. The search for new objects in the discovery data is aided by analysis software similar to that used in other surveys[32] but adapted specifically to the DECam data set. The analysis software identifies candidate objects in the data set, which are verified by visual inspection of the images.

Our search methodology consists of discovery with DECam and additional follow-up at the Magellan telescope for any object moving at <2.5 arcseconds per hour (opposition distance of >50 AU or farther). Ninety trans-Neptunians between 30 AU and 50 AU were detected, but only 2012 VP_{113} was found beyond 50 AU and required follow-up. 2012 VP_{113} was discovered on 5 November 2012 UT (Universal time) moving at 1.6 arcsec per hour in right ascension. We recovered 2012 VP_{113} again on 10–11 March 2013 UT, 10–11 August 2013 UT and 28–30 October 2013 UT with IMACS on the Magellan Baade telescope. We further identified 2012 VP_{113} in archival images taken at the Canada–France–Hawaii Telescope on 22 October 2011 UT. The orbital arc[33] for 2012 VP_{113} is over two years in duration and is securely known.

Colour measurements. The physical surface colours of inner Oort cloud objects can yield information about which formation model is likely. The classical KBOs (<0.2 eccentricity with semi-major axes in the range 40–45 AU) appear to be dominated by ultra-red colours, a rare surface colour, probably implying that their surfaces are rich in organic material[34]. We therefore obtained the optical colours of 2012 VP_{113} in the Sloan *g*, *r* and *i* bandpasses at Magellan on 10 and 11 August 2013 UT. The colours were determined using typical techniques[35]. The colour results show that 2012 VP_{113} is of only moderately red colour (see Extended Data Table 3). A moderate red colour is consistent with formation in the gas giant region, similar to the presumed origin of the outer Oort cloud bodies and scattered disk and not the ultra-red dominated classical Kuiper belt[34,35]. Using our photometry, the 83-AU heliocentric distance of 2012 VP_{113}, and assuming a moderate albedo of 15% (ref. 36), we determine that 2012 VP_{113} is 450 km in diameter.

Observational bias simulation. Because minor planets are visible in reflected sunlight, there is a 4th-power drop in observed flux with increasing heliocentric distance, a very strong bias against finding distant objects. To model and ultimately correct for these biases, we constructed a simple model of our observational technique. Underlying parameters characteristic of the inner Oort cloud object orbits are assumed, and then the position and brightness of each object at a particular time is calculated. The model population is based on a range of size distributions[22] and a Gaussian scattered KBO inclination distribution[37] with a uniform eccentricity distribution and a power-law semi-major axis distribution[32]. The values of the assumed parameters are detailed in Extended Data Table 1, and are used to create the ensemble of simulated objects. We note that although we believe we have chosen a reasonable range of parameters for the size and orbital distribution of the inner Oort cloud objects, these are based entirely on extrapolations from the KBOs. Revisions are likely in the future if the size and orbital distributions of the inner Oort cloud objects deviate significantly from that of the KBOs. Once the model population is generated, any objects brighter than our survey sensitivity limit $m_r = 24.3$ and within our distance sensitivity (from 50 AU, our minimum heliocentric distance follow-up criterion, to beyond 300 AU, where we begin to be limited by slow object motion) are tallied as a function of ecliptic latitude. Given the typical ecliptic latitudes of our observed fields, this tally yields the number and orbital characteristics of the inner Oort cloud objects we should have found if our assumed distribution matches the real distribution. In our observational model, we have included our survey as well as the deepest near all-sky survey to date, which detected Sedna[21], because it is an additional constraint on the inner Oort cloud objects.

Our first goal of the bias simulation is to examine the perihelion distribution of both Sedna and 2012 VP_{113} because both objects were found with large perihelia (>75 AU) in surveys that were sensitive to objects with smaller perihelia. Figure 2 and Extended Data Table 1 describe an assumed size distribution of $q' = 5$ (similar to the bright KBOs and the large bodies of other stable populations)[22,23,38]; however, we also test size distributions with $q' = 3.5$, 4.0 and 4.5, which are found for smaller objects in some small-body populations[39]. We find that the counting statistics for objects in the 50–75 AU region are dependent on the size distribution assumed. For the size distributions of $q' = 3.5$, 4.0, 4.5 and 5.0, we find the probability of finding Sedna and 2012 VP_{113} with perihelion beyond 75 AU when the underlying size distribution extends down to 50 AU is 17%, 7%, 5% and 1%, respectively. Given that we have no knowledge of the underlying size distribution of the inner Oort cloud objects, we cannot statistically rule out the possibility that the 50–75 AU region could be populated with inner Oort cloud objects. However, it appears to have a paucity of inner Oort cloud objects compared to $q > 75$ AU, especially if the inner Oort cloud objects have a steep size distribution like that of the bright KBOs.

Our second goal for the observational simulation is to assess whether the clustering of ω near 0° found for Sedna, 2012 VP_{113} and the objects listed in Extended Data Table 2 could be attributed to a bias effect. An ω of 0° or 180° means that the perihelion of the orbit is within the ecliptic plane. Most eccentric bodies are found near perihelion where they are brightest, so this would suggest that surveys restricted to the ecliptic plane should have a bias for finding objects with ω around 0° or 180°. We can reject this bias as an explanation of the observed ω trend for two reasons. First, any bias for $\omega = 0^\circ$ (meaning that at perihelion the object crosses the ecliptic moving southward) is the same as the bias for $\omega = 180^\circ$ (meaning that at perihelion the object crosses the ecliptic moving northward) because observational discovery surveys have no bias against direction of motion at this level. Because no objects were found with $\omega \approx 180^\circ$ and all had $\omega \approx 0^\circ$, the ω clustering is already inconsistent with any observational effect. Second, the surveys that found the objects with clustered ω were often off-ecliptic or all-sky surveys, which would not have a bias for $\omega = 0^\circ$ or 180°. Extended Data Table 2 shows the discovery ecliptic latitude *b* of the objects. In our observational simulations, we find that the $\omega = 0^\circ$ or 180° discovery bias is only significant when discovery surveys probe $|b| < 10^\circ$, which is true for only about half of the objects listed. Even when this bias is present, it should affect $\omega = 0^\circ$ and 180° equally, for the reasons discussed above. Thus, we know of no observational bias which could explain why all objects with $q > 30$ AU and $a > 150$ AU would have $\omega \approx 340^\circ \pm 55^\circ$ and none have $90^\circ < \omega < 270^\circ$.

Dynamical simulation. We used the Mercury integrator[40] to simulate the long-term behaviour of ω for the inner Oort cloud objects and objects with semi-major axes greater than 150 AU and perihelia greater than Neptune. The goal of this simulation was to attempt to explain the ω clustering. The simulation shows that for the currently known mass in the Solar System, ω for all objects circulates on short and differing timescales dependent on the semi-major axis and perihelion (for example, 1,300 Myr, 500 Myr, 100 Myr and 650 Myr for Sedna, 2012 VP_{113}, 2000 CR_{105} and 2010 GB_{17}, respectively). We illustrate an example of the ω circulation behaviour in Extended Data Fig. 2. Given that the inner Oort cloud objects and the objects listed in Extended Data Table 2 show a preference for ω near 0° but not 180°, and that the timescale for ω circulation is short (and differs between objects) compared to the age of the Solar System, we suggest that the perturber constraining ω for these objects is still present and as yet unidentified.

To test the massive perturber hypothesis as a source in constraining ω, we ran several simulations with a single body of 2–15 Earth masses in a circular low inclination orbit between 200 AU and 300 AU using the Mercury integrator. In general it was found that the ω for the inner Oort cloud objects 2012 VP_{113} and Sedna routinely librated with an amplitude of about $\pm 60^\circ$ around $\omega = 0^\circ$ for billions of years. The librating behaviour of ω for 2012 VP_{113} with an additional body of 5 Earth masses at 210 AU is illustrated in Extended Data Fig. 3, where 2012 VP_{113} spends only 3% of its time in the $90^\circ < \omega < 270^\circ$ region. Sedna spent 1% of its time in this region. For the low-*i* super-Earth simulations, the lower-perihelion objects did not librate for long periods as did 2012 VP_{113} and Sedna and spent 30% to 50% of their time with $90^\circ < \omega < 270^\circ$. We also ran simulations with highly inclined Neptune mass bodies at about 1,500 AU and found most objects exhibiting short ω librations, which suggests some interesting potential future simulation prospects. Very few dynamical simulations of inner Oort cloud object formation have considered the distribution of the argument of perihelion for inner Oort cloud objects, and so far none have produced a population that is asymmetric when comparing $\omega = 0^\circ$ to $\omega = 180^\circ$. Possible strong stochastic events might create asymmetric populations, but this needs to be confirmed through future simulations. We note that the planet configurations we tested are not unique and there are likely to be many possible orbital patterns for an unseen perturber that could produce a ω constraint among the most distant bodies in the Solar System[41,42].

31. Diehla, T. The Dark Energy Survey Camera (DECam). *Phys. Proc.* (*Proc. 2nd Int. Conf. on Technology and Instrumentation in Particle Physics, TIPP 2011*) **37,** 1332–1340 (2012).
32. Trujillo, C. A., Jewitt, D. C. & Luu, J. X. Properties of the trans-Neptunian belt: statistics from the Canada-France-Hawaii telescope survey. *Astron. J.* **122,** 457–473 (2001).
33. Bernstein, G. & Khushalani, B. Orbit fitting and uncertainties for Kuiper belt objects. *Astron. J.* **120,** 3323–3332 (2000).
34. Doressoundiram, A., Boehnhardt, H., Tegler, S. C. & Trujillo, C. in *The Solar System Beyond Neptune* (eds Barucci, M. A., Boehnhardt, H., Cruikshank, D. P., Morbidelli, A. & Dotson, R.) 91–104 (2008).

©2014 Macmillan Publishers Limited. All rights reserved

35. Sheppard, S. S. The colors of extreme outer Solar System objects. *Astron. J.* **139,** 1394–1405 (2010).
36. Stansberry, J. *et al.* in *The Solar System Beyond Neptune* (eds Barucci, M. A., Boehnhardt, H., Cruikshank, D. P., Morbidelli, A. & Dotson, R.) 161–179 (2008).
37. Gulbis, A. A. S. *et al.* Unbiased inclination distributions for objects in the Kuiper belt. *Astron. J.* **140,** 350–369 (2010).
38. Sheppard, S. S. & Trujillo, C. A. The size distribution of the Neptune Trojans and the missing intermediate-sized planetesimals. *Astrophys. J.* **723,** L233–L237 (2010).
39. Petit, J.-M., Kavelaars, J. J., Gladman, B. & Loredo, T. in *The Solar System Beyond Neptune* (eds Barucci, M. A., Boehnhardt, H., Cruikshank, D. P., Morbidelli, A. & Dotson, R.) 71–87 (2008).
40. Chambers, J. E. *Mercury: a Software Package for Orbital Dynamics* (Astrophysics Source Code Library, 2012).
41. Lykawka, P. S. & Mukai, T. An outer planet beyond Pluto and the origin of the trans-Neptunian belt architecture. *Astron. J.* **135,** 1161–1200 (2008).
42. Lykawka, P. S. & Ito, T. Terrestrial planet formation during the migration and resonance crossings of the giant planets. *Astrophys. J.* **773,** 65 (2013).

©2014 Macmillan Publishers Limited. All rights reserved

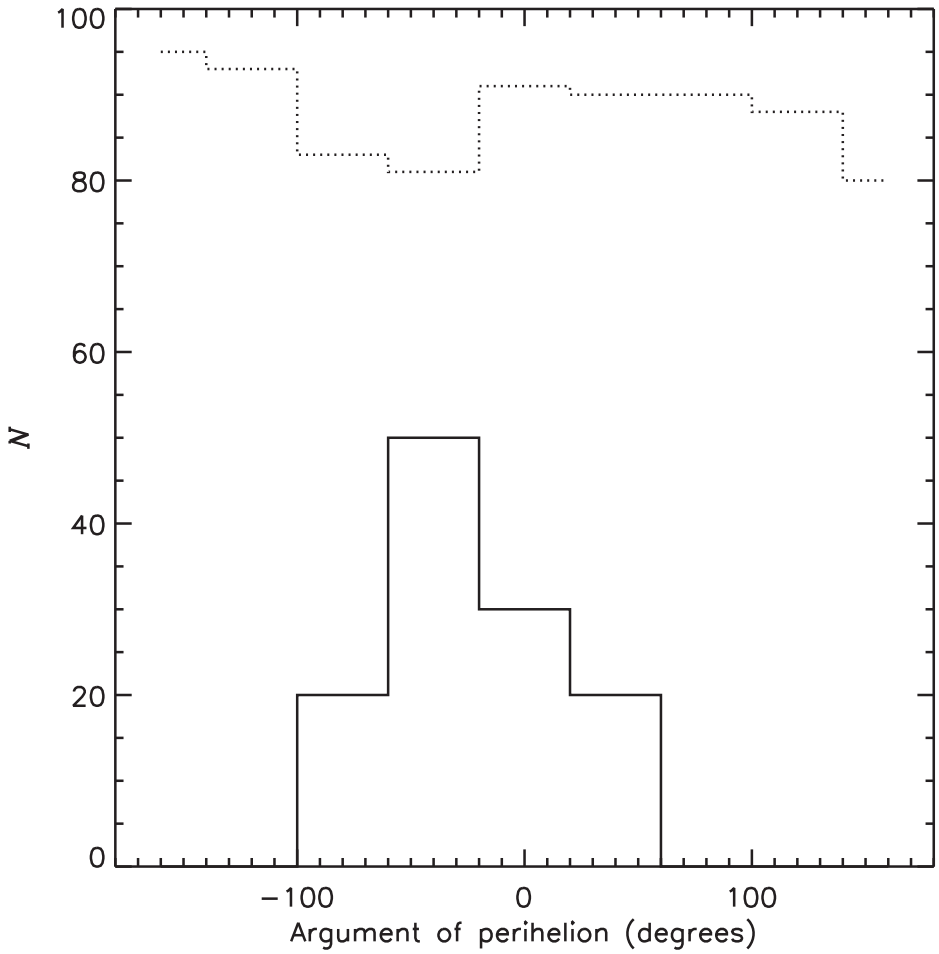

Extended Data Figure 1 | Histogram of ω for minor planets with $q > 30$ AU. This is similar to Fig. 3 but in histogram form. The bodies with $a > 150$ AU are shown as a black line (multiplied by a factor of ten for clarity) and bodies with $a < 150$ AU are shown as a dotted line. The two distributions differ according to Kuiper's test with a significance of 99.9%.

©2014 Macmillan Publishers Limited. All rights reserved

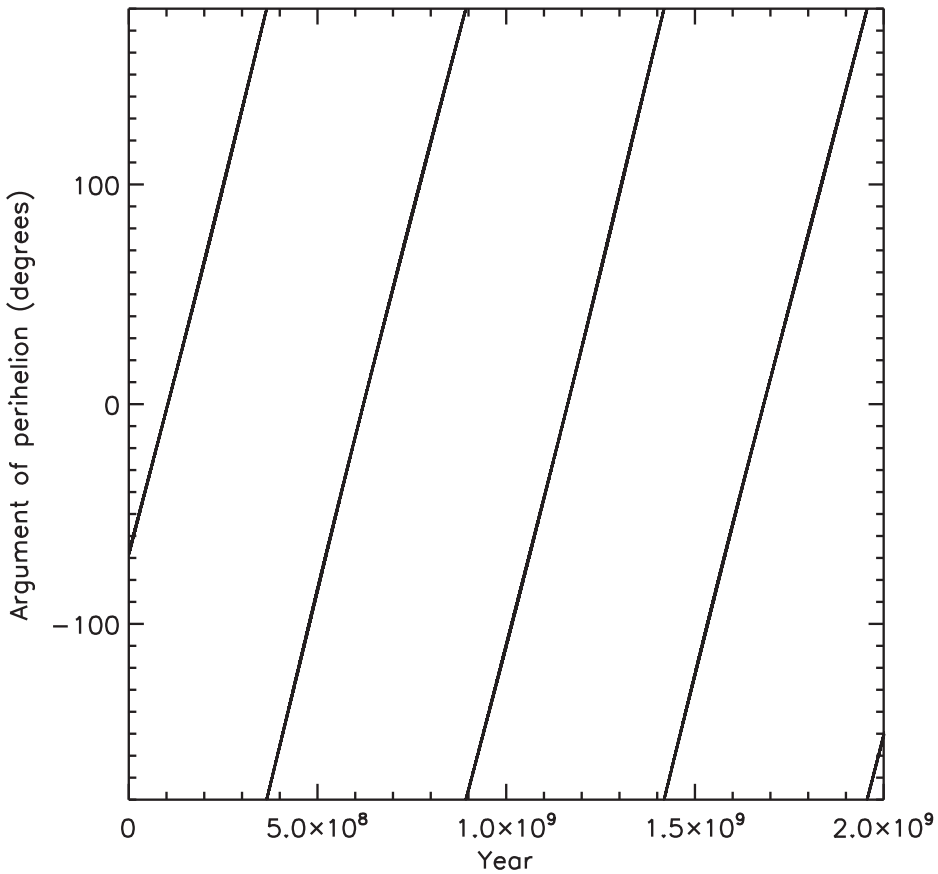

Extended Data Figure 2 | The ω cycling of 2012 VP_{113} in the current Solar System. We note that over the course of 500 Myr, the argument of perihelion ω moves uniformly across all values. All inner Oort cloud Objects (Table 1) and other distant objects (Extended Data Table 2) are expected to exhibit this behaviour on differing timescales, so the observation that all are restricted to ω near 0° is inconsistent with the current dynamical environment in the Solar System. Because these are simulated plots, there are no error bars associated with data points.

©2014 Macmillan Publishers Limited. All rights reserved

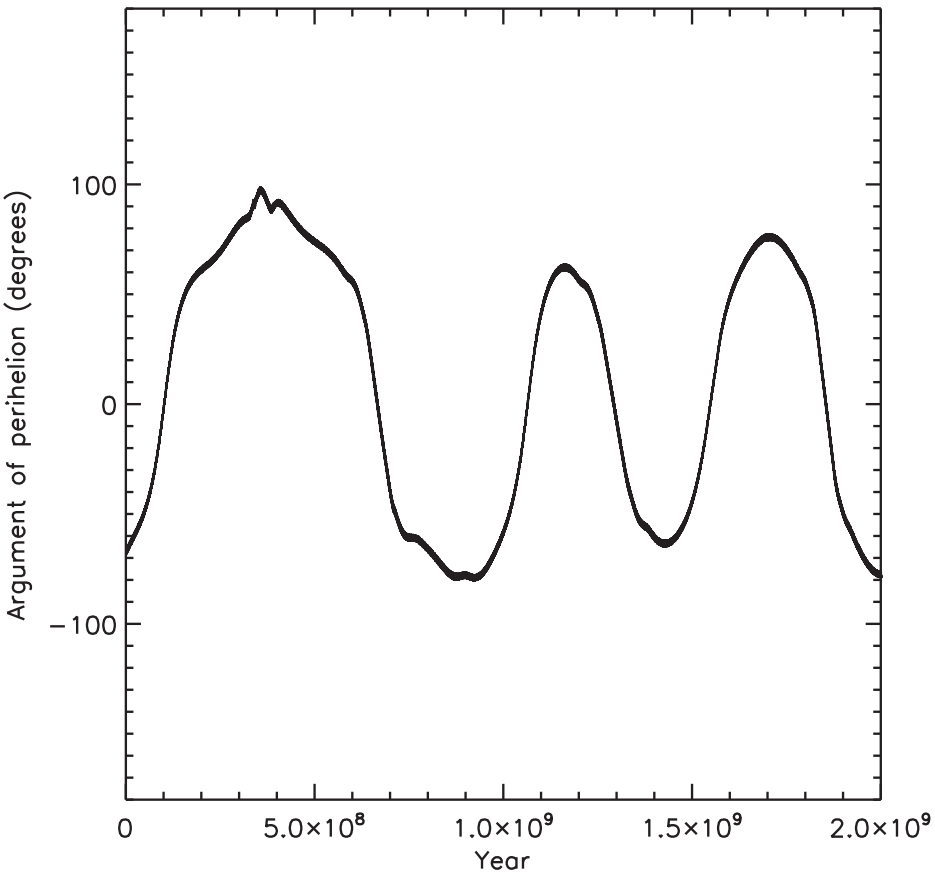

Extended Data Figure 3 | The libration of ω for 2012 VP_{113} with an assumed object five times the mass of Earth at 210 AU. 2012 VP_{113} librates about $\omega = 0^\circ$ for most of the duration of the Solar System. This behaviour could explain why the two inner Oort cloud Objects (Table 1) and all objects with semi-major axes greater than 150 AU and perihelia greater than Neptune's (Extended Data Table 2) have $\omega \approx 0^\circ$. The choice of mass and orbit of the perturber is not unique. Many possible distant planetary bodies can produce the pictured Kozai resonance behaviour, but the currently known Solar System bodies cannot. These are simulated plots, so there are no error bars associated with data points.

©2014 Macmillan Publishers Limited. All rights reserved

Extended Data Table 1 | Model parameters for the $q' = 5$ inner Oort Cloud observational bias and population study

Parameter	Value	Description
ρ	1000 kg m^{-3}	Density
N	1.5×10^8	Number of objects
r_{min}	25 km	Minimum radius
r_{max}	4000 km	Maximum radius
a_{min}	200 AU	Minimum semi-major axis
a_{max}	800 AU	Maximum semi-major axis
q_{min}	50 AU, 75 AU	Minimum perihelion
e_{min}	0.5	Minimum eccentricity
q'	5.0	Size distribution power law exponent
a	1	Semi-major axis distribution power law exponent
p_r	0.15	Albedo in r filter
σ_i	6.9°	Sigma for Gaussian inclination distribution
μ	19.1°	Mean for Gaussian inclination distribution

Size distributions of $q' = 3.5$, 4.0 and 4.5 were also studied, with all parameters identical except that $N = 4 \times 10^6$, $N = 1 \times 10^7$ and $N = 4 \times 10^7$, respectively. The population mass varies greatly with the model assumed, $M = 5$, 1/30, 1/40 and 1/80 Earth masses for $q' = 3.5$, 4.0, 4.5 and 5.0.

©2014 Macmillan Publishers Limited. All rights reserved

Extended Data Table 2 | Orbital elements of extreme Solar System bodies

Object	b (deg)	q (AU)	a (AU)	e	i (deg)	Ω (deg)	ω (deg)	t_p (JD)	epoch (JD)
2010 GB_{174}	17.3	48.5	365	0.87	21.536	130.60	347.4	2,433,983	2,456,600.5
2004 VN_{112}	-16.2	47.332	339	0.8602	25.5169	66.061	327.21	2,455,126	2,456,600.5
2000 CR_{105}	2.9	44.16	229	0.8077	22.7119	128.2393	316.99	2,438,937	2,456,600.5
2005 RH_{52}	12.1	39.016	153.7	0.7461	20.4676	306.193	32.66	2,452,842	2,456,600.5
2003 HB_{57}	-0.2	38.086	159.8	0.7617	15.503	197.8715	10.62	2,454,836	2,456,600.5
2007 TG_{422}	-17.4	35.581	547	0.9349	18.5794	112.981	285.82	2,453,693	2,456,600.5
2002 GB_{32}	2.5	35.339	207.1	0.8293	14.1880	177.0275	36.87	2,456,718	2,456,600.5
2007 VJ_{305}	7.4	35.203	194.3	0.8188	11.982	24.385	338.56	2,453,762	2,456,600.5
2010 VZ_{98}	-4.5	34.31	157.9	0.782	4.5090	117.47	313.7	2,461,724	2,456,600.5
2001 FP_{185}	0.1	34.231	218.4	0.8432	30.7920	179.3438	6.71	2,452,968	2,456,600.5

This includes all bodies with perihelia greater than 30 AU and semi-major axes greater than 150 AU, except for the two inner Oort cloud objects listed in Table 1. The JPL Horizons heliocentric orbital elements are given as semi-major axis (a), eccentricity (e), inclination (i), longitude of ascending node (Ω), argument of perihelion (ω), and perihelion distance (q), which has been derived from a and e. Time of perihelion (t_p) and epoch are specified in terms of Julian Date (JD). The precision to which quantities are known is reflected in the number of significant digits. As discussed in the text, the first three objects may have origins similar to those of the inner Oort cloud objects, although their perihelia are far lower than that of either Sedna or 2012 VP_{113}. We also show the discovery ecliptic latitude b of the objects because the bias for finding bodies with $\omega = 0^\circ$ or 180° is relatively low when $|b| > 10^\circ$ (Methods).

©2014 Macmillan Publishers Limited. All rights reserved

Extended Data Table 3 | Colours of 2012 VP_{113}

Quantity	Value
Sloan Colours	
r	23.35 ± 0.02
$g - r$	0.70 ± 0.05
$r - i$	0.32 ± 0.04
Johnson-Kron-Cousins Colours	
R	23.10 ± 0.03
$B - R$	1.44 ± 0.05
$V - R$	0.52 ± 0.04
$R - I$	0.53 ± 0.04

These colours yield a spectral slope of 13 ± 2% per 100 nm and a reduced magnitude in the R-band of 3.8 ± 0.04. The reduced magnitude suggests that 2012 VP_{113} is about 450 km in diameter, assuming a moderate albedo of 15%.

©2014 Macmillan Publishers Limited. All rights reserved